sustainability

MDPI

Article

Effect of Temperature and Humidity on the Synthesis of Alkali-Activated Binders Based on Bottom Ash from Municipal Waste Incineration

Pietro C. D. Tortora [1], Alex Maldonado-Alameda [2], Jofre Mañosa [2], Alex C. Quintero-Payan [2], Cristina Leonelli [1], Isabella Lancellotti [1] and Josep M. Chimenos [2,*]

[1] Department of Engineering "Enzo Ferrari", University of Modena and Reggio Emilia, 41125 Modena, Italy; pietrotortora883@hotmail.it (P.C.D.T.); cristina.leonelli@unimore.it (C.L.); isabella.lancellotti@unimore.it (I.L.)
[2] Departament de Ciència de Materials i Química Física, Universitat de Barcelona, 08028 Barcelona, Spain; alex.maldonado@ub.edu (A.M.-A.); jofremanosa@ub.edu (J.M.); alex.quintero@ub.edu (A.C.Q.-P.)
* Correspondence: chimenos@ub.edu

Abstract: Weathered bottom ash (WBA) from municipal solid waste incineration is a calcium aluminosilicate-rich material mainly used in construction and civil engineering as a secondary aggregate. However, its use is also being considered as a precursor in the manufacture of alkali-activated binders (AA-WBA). This preliminary research aimed to deepen understanding of the potential use of WBA (>8 mm fraction) as the sole precursor of alkali-activated binders. To gain better knowledge of this material, the physicochemical, mechanical, and environmental properties of AA-WBA binders were evaluated. In addition, the effect of curing temperature (25 °C, 45 °C, 65 °C, and 85 °C) and humidity conditions (oven and climate chamber) were assessed. The results of this study revealed that temperature and humidity conditions play a fundamental role during the early formation stages of AA-WBA binders. Maximum compactness and compressive strength (29.8 MPa) were obtained in the sample cured at 65 °C in the oven and room humidity. At higher temperatures (85 °C), a substantial decrease in mechanical strength (21.2 MPa) was observed due to a lower cohesion of the binder phases. Curing in the climate chamber led to an increase in humidity, and therefore a decrease in compressive strength. Finally, lower porosity and longer curing time substantially decreased the heavy metals and metalloid leaching concentration of AA-WBA binders.

Keywords: alkali-activated binders; incineration bottom ash; MSWI; weathered bottom ash; alternative cement; waste valorization

Citation: Tortora, P.C.D.; Maldonado-Alameda, A.; Mañosa, J.; Quintero-Payan, A.C.; Leonelli, C.; Lancellotti, I.; Chimenos, J.M. Effect of Temperature and Humidity on the Synthesis of Alkali-Activated Binders Based on Bottom Ash from Municipal Waste Incineration. *Sustainability* **2022**, *14*, 1848. https://doi.org/10.3390/su14031848

Academic Editor: Dino Musmarra

Received: 14 December 2021
Accepted: 4 February 2022
Published: 6 February 2022

1. Introduction

Portland cement (PC) is one of the largest contributors to climate change worldwide. The high demand and thermal processes related to clinker production have made PC a major CO_2 emissions source. It is estimated that, worldwide, the cement sector causes between 5 and 7% of global CO_2 emissions, and consumes 3% of global primary energy [1]. Therefore, the cement industry needs to move forward in accordance with the Paris Agreement on climate change and undergo significant changes, by which it improves thermal processes and looks for alternative cement-based materials. Alkali-activated binders (AABs) are one of the most interesting options given their performance and low-carbon manufacturing process [2]. These alternative binders are obtained at temperatures below 100 °C by reacting a strongly alkaline activator with a solid precursor powder that is rich in aluminosilicates, resulting in a binder material comparable to PC [3]. The alkali activation process starts with the dissolution of the aluminates and silicates of the precursor in an alkaline medium, which leads to the nucleation of new phases, called gelation. Depending on the calcium content, two types of gel structure can be formed: calcium aluminosilicate hydrate (CASH), the gel for high-calcium systems, and sodium aluminosilicate hydrate (NASH), the gel for

low-calcium systems [4]. Recent studies have found the likely coexistence of both NASH and CASH structures, known as (C,N)ASH gel [5–7]. After a proper activation process, a gel is formed. Its nature and final structure strongly depend to a large extent on the CaO content of the precursor [6], the alkaline activator [8], and the curing temperature [9]. Another advantage of AABs is the possibility of using a wide range of industrial waste as raw materials, which encourages the zero-waste principle within a circular economy, promotes more sustainable processes, and leads to less use of natural resources. However, new secondary resources must be found and/or studied in greater depth to supply the current worldwide demand for binders [10]. Among these secondary resources, incineration bottom ash (IBA) from waste-to-energy (WtE) facilities stands out due to its potential as an alkali-activated precursor.

The appropriate management of municipal solid waste (MSW) is essential to avoid negative impacts on ecosystems, biodiversity and health [11]. Faced with this threat, the European Union (EU) has adopted measures to improve waste management and move towards a circular economy. One measure is the restriction of landfilling of waste to a minimum for all member states. Moreover, the EU promotes the adoption of technologies that incorporate waste valorization into the production cycle, as proposed in the commitments made by the EU in the 2030 Agenda for Sustainable Development. In this way, MSW emerges as a potential raw material instead of waste to be landfilled. Many EU countries consider that MSW incineration is an opportunity to recover energy that allows them to reduce the mass and the volume of waste [12]. Nonetheless, the MSW combustion process generates new solid wastes, namely, incineration bottom ashes (IBA) and air pollution control residues (APC). The main solid output from the combustion process is IBA, the non-combustible materials that remain in the furnace, which account for about 80 wt.% of all incinerated MSW [13]. In Europe, around 18 Mt of IBA are generated each year [14]. Part of IBA is valorized as a secondary granular material in civil engineering after a proper stabilization process. The resulting material, known as weathered bottom ash (WBA), consists mainly of heterogeneous minerals [15]. Some legal and technological barriers hamper the valorization of WBA in many countries. Consequently, it is put in landfills [14,16]. Therefore, the scientific community continues to study potential applications for the valorization of IBA, to increase its value-added potential. Some of these potential applications focus on the use of IBA as a precursor in alkali-activation technology [17–22].

IBA is a silica-rich material, mainly owing to the high content of primary and secondary glass [13,23]. It contains significant amounts of calcium and aluminum oxides, which are also required to formulate AABs [24]. Furthermore, IBA contains other oxides (Na_2O, K_2O, etc.) and a small amount of heavy metals and metalloids, mainly in the finest particle size fractions [25]. The use of IBA as an alkali-activated precursor could be a potential alternative to its common reuse as secondary building material, due to its composition [26]. Moreover, the alkali activation of IBA could contribute to a circular economy, favoring the zero-waste principle and being a sustainable alternative to PC, at least for non-structural building components.

Although the literature is scarce [24], the use of IBA in the formulation of alternative cement to PC has been investigated mostly as a partial precursor, in small percentages, mixed with other cement precursor materials such as granular blast furnace slag (GBFS), metakaolin (MK), coal-fired power plants' fly ash (FA), or PC [27–34]. The mechanical characterization (up to 60 MPa compressive strength) showed the possibility of obtaining alkali-activated binders or mortars, depending on the precursors that are used and the IBA content. However, literature on the formulation of AABs using IBA as a sole precursor is even more scarce than research into its use as a partial precursor [18–20,35]. Most of these studies demonstrated the unconventionality of using IBA as a unique precursor in alkali-activation technology. This is probably due to the presence of metallic aluminum and soluble salts as well as the heterogeneity of IBA. However, practically all the studies cited above used the entire fraction of IBA (0–30/40 mm) as a precursor. Most soluble salts and heavy metals and metalloids are concentrated in the finest fractions [13]. Moreover,

some waste-to-energy plants recover non-ferrous metals from IBA to recycle metallic aluminum. However, the recovery process is regarded as unsuccessful for particles smaller than 8 mm [13]. The presence of metallic aluminum affects the mechanical behaviour of AABs, since it leads to a porosity increase due to the generation of hydrogen gas from the reaction between aluminum contained in IBA and the alkaline activators [36]. In contrast, the coarser fractions of IBAs are richer in glass (cullet) from containers and there is greater availability of SiO_2 for gelation reactions [13,19]. As a result, there is currently a tendency to use only the coarse fraction of IBAs as a precursor in the formulation of AABs [22,35,37], from the technical and environmental perspective. In either case, alkali activation using a combination of NaOH and Na_2SiO_3 (waterglass) as alkaline activators [38,39] has proven efficient for precursors with high calcium contents. All the studies demonstrated the viability of obtaining hardened cementitious binders with different final properties. Microstructural analysis of the binders revealed the formation of C(A)SH and NASH gels. While sodium silicate-activated precursors tend to gain strength more slowly than sodium hydroxide-activated precursors, the former show better long-term mechanical strengths [40,41]. Most of the studies of curing of IBA-based AABs were carried out under similar temperature and relative humidity (RH) conditions, based on keeping the specimens at room temperature and RH of approximately 95% $\pm$ 5% until testing. Notably, the high content of calcium and glassy phases in IBA facilitates alkaline activation at room temperature. However, research on the alkaline activation of other calcium-rich systems (e.g., GBFS) reported that high-temperature curing increases the rate of microstructure formation and may affect mechanical resistance [42,43].

This research is part of a larger project to study the potential use of WBA as a sole precursor in the formulation of alkali-activated binders [19,20,22]. Some issues, such as the most suitable particle size fraction of WBA, the alkaline concentration of the activator, the ratio between activators, or the precursor–activator ratio, have already been optimized to obtain the best mechanical and environmental properties. However, other technical aspects related to curing conditions should be studied to improve the performance and requirements of the formulated binders. Accordingly, this study approaches the development of alkali-activated binders using the coarse fraction (>8 mm) of WBA (AA-WBA). The novelty mainly lies in assessing the effect of the curing temperature and relative humidity on the final properties of AA-WBA binders. This is the first time that a study has focused on the influence of curing conditions in AABs formulated with WBA as a sole precursor. In addition, the environmental performance of AA-WBA binders was evaluated through the EN 12457-4 granular leaching test.

2. Materials and Methods

2.1. Materials

The WBA used in this research was provided by VECSA, a company responsible for the conditioning and recovery of IBA from the incineration plant of SIRUSA in Tarragona (Spain). The SIRUSA facility has a capacity of 144 kt of MSW per year. This MSW is mainly comprised of household rubbish, with a small input from commercial vendors. The facility produces about 32 kt of fresh IBA each year [44]. IBA produced in the SIRUSA facility is treated in a conditioning plant (VECSA), where valuable metals are recovered, lightweight unburned materials are removed, and the mineral fraction is sieved to obtain a grading envelope (0–30 mm). Then, the conditioned IBA is stabilized in the open for 2–3 months under natural weathering to obtain WBA. The collected WBA sample (50 kg) was dried at 105 °C for 24 h and subsequently sieved to obtain a 8–30-mm fraction. This coarse fraction represents approximately 30 wt.% of the total sample and is mainly composed of ceramic materials and primary and secondary glass [13]. Afterwards, a magnet (Nd; 0.485 T) was used over the quartered dry sample (>8 mm) to remove magnetic particles. Then, the sample was crushed and ground in a RETSCH BB 50 jaw crusher to obtain a particle size powder below 80 µm.

The elemental composition of WBA powder was assessed by X-ray fluorescence (XRF) analysis with a Panalytical Philips PW 2400 sequential X-ray spectrophotometer equipped with UniQuant® V5.0 software. Major elements, expressed as their most stable oxides, are given in Table 1. The high SiO_2 content was mainly due to the presence of primary and secondary glass in WBA, while the presence of CaO and Al_2O_3 comes from fired ceramics and cementitious materials based on PC [13].

Table 1. Major elements composition (wt.%) of WBA powder (>8 mm).

SiO_2	CaO	Al_2O_3	Na_2O	K_2O	$Fe_2O_{3\ (tot)}$ *	MgO	TiO_2	Cl^-	SO_3	[1] LOI
52.08	20.72	6.35	3.38	2.09	4.12	2.43	0.65	0.54	1.07	6.10

[1] Loss on ignition at 1000 °C. * The content of iron is expressed as total iron oxide, calculated by stoichiometry from iron signal, as usual, is reported for results from XRF spectrometry analysis.

Moreover, the crystalline phases of WBA powder were determined through a Bragg–Brentano Siemens D-500 powder diffractometer device with CuK_α radiation. The X-ray diffraction (XRD) pattern identified the presence of quartz (SiO_2) and calcite ($CaCO_3$) as the main crystalline phases. Furthermore, dolomite ($CaMg(CO_3)_2$), akermanite ($Ca_2Mg(Si_2O_7)$), anhydrite ($CaSO_4$), microcline ($KAlSi_3O_8$), and muscovite ($KAl_2(AlSi_3O_{10})(OH)_2$) were also identified as minor crystalline phases. The large halo between 20° and 30° was attributed to the vitreous nature of the coarse fraction of WBA.

The alkali activator used in this study was a mixture of a commercial Na_2SiO_3 solution (Scharlab S.L.) with molar ratio SiO_2/Na_2O = 3.22 (26.44 wt.% of SiO_2 and 8.21 wt.% of Na_2O; ϱ = 1.37 g·cm^{-3}) and a NaOH 6 M solution prepared using NaOH pearls (Labbox Labware S.L.; purity > 98%) dissolved in deionized water (ϱ = 1.20 g·cm^{-3}).

2.2. Alkali-Activated WBA (AA-WBA) Binder Preparation

Table 2 summarizes the mix formulation, chemical composition of the alkaline activator solution, and curing conditions of AA-WBA binders. The NaOH concentration (6 M) and Na_2SiO_3/NaOH mass ratio (80/20) remained constant in all formulations, based on previous studies. The alkaline activator-to-precursor mass ratio was fixed at 0.8, considering the proper workability of fresh AA-WBA pastes during mixing and casting processes. The formulation of AA-WBA binders was carried out following the procedure described by Maldonado-Alameda et al. [22], where the optimal formulation of alkali-activated WBA was found using the coarse fraction (>8 mm).

Table 2. Mix proportion and alkaline activator chemical composition of AA-WBA binders.

Reference	Precursor	Activator		Curing Temperature	
	WBA (>8 mm)	NaOH 6M (wt.%) [a]	Na_2SiO_3 (wt.%) [a]	0–3 Days (Oven; Sealed Plastic Bag)	3–28 Days (Climatic Chamber; 95 ± 2% RH))
AA-WBA-25 °C	100	16	64	25 °C	25 °C
AA-WBA-45 °C	100	16	64	45 °C	25 °C
AA-WBA-65 °C	100	16	64	65 °C	25 °C
AA-WBA-85 °C	100	16	64	85 °C	25 °C

[a] Concerning the WBA.

The preparation started by mixing the alkaline activator solution for 3 min. Then, the solid was gradually added into the liquid (alkaline activator) for 2 min at 470 rpm to favor the dissolution of reactive phases. Subsequently, the whole mixture was stirred for 3 min at 760 rpm. The resulting fresh pastes were cast into 25 × 25 × 25-mm^3 cubic molds and sealed in plastic bags. Subsequently, the specimens were subjected to different curing temperatures (25, 45, 65, and 85 °C) for 3 days in a stove. After 3 days, the specimens were demolded and the curing stage continued in a climatic chamber at 25 °C and 95 ± 2%

RH. Finally, after 28 days of curing, the specimens were measured and weighed before subsequent testing and analysis to determine the chemical, physical, mechanical, and environmental properties of the AA-WBA binders. Nine cubic-shaped specimens were prepared for each curing temperature.

Once the optimal curing temperature was determined, another formulation was carried out to assess the effect of relative humidity conditions. In this case, the curing process was entirely conducted (28 days) at the optimum curing temperature in a climate chamber, where the relative humidity conditions (95 ± 2% RH) were kept constant.

2.3. Characterization of Alkali-Activated WBA Binders (AA-WBA)

The hydrolytic stability of each formulation was assessed by placing a dried specimen in boiling water for 20 min [45]. Then, a visual evaluation was conducted to determine the resistance to dissolution in water. After that, the specimens were dried in a desiccator with silica gel until they reached a constant weight. Finally, the specimens were weighed to determine the mass loss and to quantify the chemical stability and resistance to dissolution.

Selective chemical extraction was conducted to eliminate any ambiguity between the C(A)SH and NASH gels [5]. Accordingly, a specimen for each cured temperature was subjected to the salicylic acid/methanol (SAM) [46] and HCl extractions [47] to determine the C(A)SH and NASH content. As previously described, the alkali-activation of precursors with high calcium content (i.e., WBA) leads to the formation of C(A)SH and NASH gels [20,22]. However, when both formed gels coexist, it is difficult to properly elucidate C(A)SH using X-ray diffraction (XRD) or Fourier transform infrared spectroscopy (FTIR). In this case, SAM and HCl extraction were used to dissolve the C(A)SH phases and NASH phases, respectively. The calcium-containing phases were dissolved in the SAM medium, while the rest of the mineral phases remained in the insoluble residue. The SAM extraction procedure consisted of mixing 1 g of powder sample with salicylic acid (6 g) and methanol (40 mL) for 1 h. The mixture was subsequently filtered (20-µm pore size) to obtain the insoluble residue. The HCl extraction consisted of stirring 1 g of powder sample with 250 mL of HCl (1:20) solution for 3 h, followed by filtration (20-µm pore size). Then, the insoluble residues were washed with deionized water and dried until constant weight. The percentage of weight loss due to SAM and HCl extraction was calculated by weighing the insoluble residue.

The main crystalline phases of AA-WBA binders were determined using a Bragg–Brentano Siemens D-500 powder diffractometer device with CuK_{α} radiation. The vibrational energies of the most characteristic bonds in AA-WBA binders were identified through Fourier transform infrared spectroscopy (FTIR) in attenuated total reflectance mode (ATR). Spectrum Two^{TM} equipment from Perkin–Elmer was configured to conduct measurements with an average of 32 scans in the range of 4000–400 cm^{-1} (resolution of 4 cm^{-1}). Subsequently, the FTIR spectra deconvolution was performed in the mid-wavenumber region (1300–800 cm^{-1}) through Origin software to reveal the overlap of the fundamental band. Gaussian functions were added to adjust the shape of the spectra. The fitting with Gaussian functions was combined with the self-fitting function of the computer software. Finally, the microstructure of AA-WBA binders was observed using a scanning electron microscopy (SEM) device (ESEM FEI Quanta 200).

Mechanical properties at 28 days of curing were determined through the compressive strength (σ_c) test of three cubic samples for each formulation. An Incotecnic MULTI-R1 device equipped with a 20-kN load cell was used. A progressive load was applied until fracture (loading rate of 240 $kg{\cdot}s^{-1}$), according to UNE-EN 196-1. In addition, density and porosity were determined on some specimens using an Accypy1330 Micromeritic gas pycnometer (He).

Finally, the potential release of heavy metals and metalloids of AA-WBA specimens was evaluated through a granular leaching test following European standard EN 12547–4. A Perkin–Elmer ELAN 6000 ICP mass spectrometry (ICP-MS) device was used to analyze

the heavy metals and metalloids in the eluates (As, Ba, Cd, Cr, Cu, Hg, Mo, Pb, Ni, Se, Sb, and Zn). Two replicas per raw material and AA-WBA binders' formulation were conducted.

3. Results and Discussion

3.1. Effect of Curing Temperature

The hydrolytic stability test in boiling water showed that AA-WBA binders do not disaggregate and remain cohesive (Figure 1). The weight loss after the test was less than 2 wt.% in all tested specimens, which was not enough to affect the structural consistency of AA-WBA binders. This indicates that the binders' consistency was due to the alkali activation of the WBA and not to waterglass (Na_2SiO_3) drying, since waterglass is soluble in water.

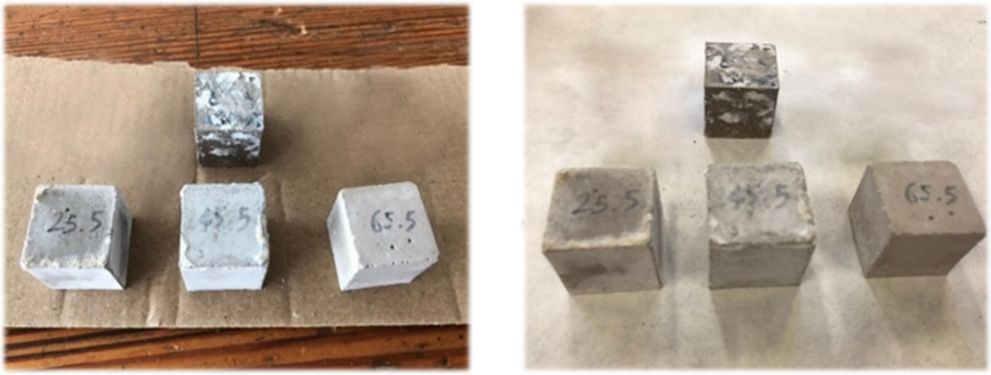

(**a**) (**b**)

Figure 1. Hydrolytic stability determined in boiling water (20 min): (**a**) AABs specimens before the test; (**b**) AABs specimens after the test.

Selective extractions with SAM and HCl were carried out to study the formation of the binder phases in the formulations. Table 3 summarizes the dissolved mass percentage for each sample according to the chemical extraction performed. The dissolved mass of the AA-WBA binders significantly increased compared with WBA. This was probably due to the neoformation of CSH and (N,C)ASH gels [5,45]. The mass dissolved in chemical extractions increased as the curing temperature increased, to reach a maximum in the sample at 65 °C. The sample at 85 °C presented a slight decrease in dissolved mass. The difference in the mass dissolved percentage between WBA and AA-WBA binders, as well as the gap between both chemical extractions, indicates that most of the formed phases contained calcium (CSH and/or CASH). Consequently, the presence of sodium gel phases (NASH) was minor. In addition, the results showed that an increase in curing temperature led to an increase of CSH/CASH gels, while the formation of NASH gel remained constant regardless of the curing temperature.

Table 3. Results of the chemical extractions with SAM and HCl of the AA-WBAs resulting from each of the curing temperatures.

	Mass Dissolved with SAM (wt.%)	Mass Dissolved with HCl (wt.%)	Gap between Both Extractions
WBA	4.60	28.5	23.9
AA-WBA-25 °C	12.8	34.8	22.0
AA-WBA-45 °C	14.8	36.5	21.7
AA-WBA-65 °C	18.8	40.4	21.6
AA-WBA-85 °C	15.1	37.0	21.9

Table 4 summarizes the crystalline phases in AA-WBA binders depending on curing temperature. The main phases identified in the precursor (quartz, calcite, and dolomite) remained in all the samples. This demonstrated the nonreactive nature of these phases towards alkaline activation. Accordingly, no significant differences were observed in the XRD patterns obtained for the specimens cured at different temperatures. The disappearance of the muscovite, akermanite, and microcline peaks was only observed in the specimen cured at 85 °C. Gaylussite ($Na_2Ca(CO_3)_2{\cdot}5H_2O$) and pirssonite ($Na_2Ca(CO_3)_2{\cdot}2H_2O$) were also detected in all formulations, which indicates the exchange of cations between the WBA and the activated alkaline solution [31]. Both carbonate phases are formed in early stages and have been reported in alkali-activated materials using bottom ash and slags [45,48]. The presence of albite ($NaAlSi_3O_8$) was also detected in all specimens. Its presence was more significant with increasing curing temperature. The origin of albite could be related to the NASH gel [31], as a result of the reaction between sodium introduced as an activator and the aluminosilicate mineral phases contained in the WBA. Calcium silicate hydrate ($Ca_6Si_3O_{12}{\cdot}H_2O$) was identified in all formulations as the main CSH phase. Gehlenite ($Ca_2Al(AlSi)O_7$) was also found in all formulations, and is associated with the secondary products formed from calcium silicate hydrate (CASH) gel [22,49], as a newly formed phase in alkaline activation. Kanemite, which is attributed to alkali–silica reaction products, was detected in AA-WBA-45 and AA-WBA-65 samples. Finally, franzinite ($(Na,Ca)_7(Si,Al)_{12}O_{24}(SO_4,OH,CO_3)_3{\cdot}H_2O$), cancrinite ($Na_6Ca_2Al_6Si_6O_{24}(CO_3)_2{\cdot}2H_2O$), and boggsite ($(Ca, Na, K)_{11}Si_{78}A_{l18}O_{192}{\cdot}70H_2O$) evidenced the formation of (N,C)ASH gels.

Table 4. Crystalline phases in AA-WBA binders depending on curing temperature.

Identified Phase	PDF	Formulations			
		AA-WBA-25 °C	AA-WBA-45 °C	AA-WBA-65 °C	AA-WBA-85 °C
Albite	01-083-1609	✓	✓	✓	✓
Akermanite	01-072-2127	✓	✓	✓	✓
Boggsite	046-1350		✓		
Calcite	01-072-1937	✓	✓	✓	✓
Calcium Silicate Hydrate	014-0035	✓	✓		
Calcium Silicate Hydrate	011-0507			✓	✓
Cancrinite	046-1332	✓			
Dolomite	01-079-1342	✓	✓	✓	✓
Franzinite	030-1170	✓			
Gaylussite	01-074-1235	✓	✓	✓	✓
Gehlenite	01-079-2422	✓	✓	✓	✓
Kanemite	025-1309		✓	✓	
Quartz	01-083-0539	✓	✓	✓	✓
Metavauxite	01-073-2346		✓		
Microcline	01-076-0918	✓	✓	✓	
Muscovite	01-077-2255	✓	✓	✓	
Pirssonite	01-070-2405	✓	✓	✓	✓

It is expected that after alkaline activation and during the gelling stage, the presence in the precursor of amorphous phases with high silica and calcium contents will lead to the formation of the amorphous gels NASH, CASH, and (N,C)ASH.

Figure 2 depicts the FTIR spectra of WBA and AA-WBA binders at different curing temperatures. Broadband in the mid-wavenumber region (at 1200–800 cm^{-1}) was observed in all cases, associated with Si-O-T (T = Si, Al) asymmetric stretching vibrations on the T-O bond [50]. The shifting of the broad peak at ~1000 cm^{-1} of WBA is attributed to the formation of new phases due to the alkaline activation of the precursor (CSH, CASH, and NASH gels) [6]. Moreover, it was found that an increase in curing temperature led to a displacement towards lower wavenumbers. This is probably due to the substitution of silicon by aluminum in the Si-O bonds and the formation of (N,C)ASH gels [47]. The peaks at 1436 cm^{-1}, 875 cm^{-1}, and 713 cm^{-1} are associated with O-C-O bonds and the stretching and bending modes of carbonates [51]. The peak at 777 cm^{-1} is attributed to Si-O-Si bonds in the quartz (SiO_2) structure [51]. It was noted that all these peaks became diffused as the curing temperature increased. Finally, the peak at 1408 cm^{-1} in the 45 °C, 65 °C, and 85 °C samples was ascribed to the formation of gaylussite ($Na_2Ca(CO_3)_2{\cdot}5H_2O$) [52], although its presence was also determined by XRD in the 25 °C sample (see Table 4). Therefore, the band probably overlapped with the more intense 1436-cm^{-1} band.

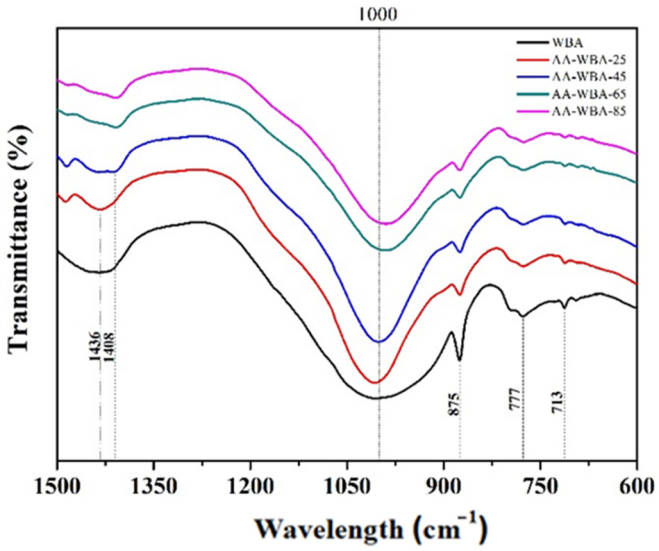

Figure 2. FTIR spectra of precursor (WBA > 8 mm) and AA-WBA binders at different curing temperatures.

Figure 3 shows the deconvoluted FTIR spectra of the WBA and AA-WBA binders to elucidate and disclose the overlap of the broadband in the mid-wavenumber region (1200–800 cm^{-1}). The broadband at 1010–994 cm^{-1} is associated with ν_3 (Si-O-T; T=Si, Al) asymmetric stretching vibrations [6,46,53]. The deconvolution of the sample cured at 25 °C (Figure 3b) shows a slight shift towards higher wavenumbers (1010 cm^{-1}) compared with WBA (1000 cm^{-1}). This is probably due to the greater incorporation of the Ca cation into the glassy structures and the formation of C(A)SH gels. Moreover, the asymmetric stretch band shifted towards the lower wavenumbers as the curing temperature increased. This is probably due to the substitution of Si atoms by Al atoms, which causes a shift of the band to lower wavenumbers due to the Al-O bond being longer than the Si-O bond. Furthermore, the bands around 1090 cm^{-1} and 1160 cm^{-1} were associated with the silicon tetrahedra Q^3 and Q^4 in a silica-rich gel. Moreover, the band around 905 cm^{-1} was assigned to the stretching vibrations of ν_2 (Si-O) and the sharp band located at 875 cm^{-1} may be attributed to C-O stretching vibrations of carbonates [54]. Finally, the small band around 865 cm^{-1} was attributed to Si-O terminal vibrations [55], which suggests incomplete polymerization.

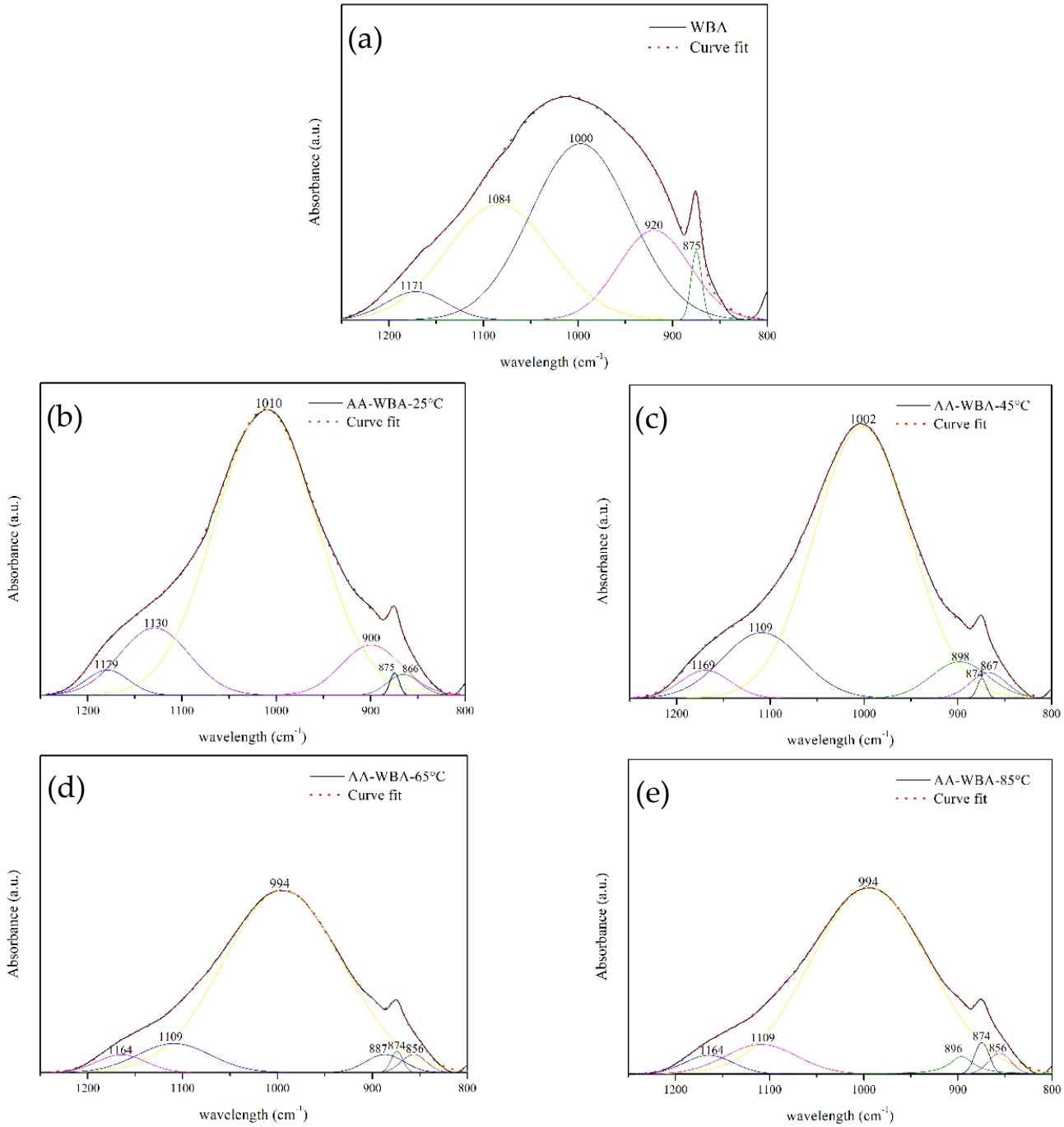

Figure 3. FTIR spectral deconvolution of the mid-wavenumber region (1300–800 cm^{-1}) for: (**a**) WBA > 8 mm; (**b**) AA-WBA-25 °C; (**c**) AA-WBA-45 °C; (**d**) AA-WBA-65 °C; (**e**) AA-WBA-85 °C.

Figure 4 shows the FTIR spectra of alkali-activated binders before and after SAM and HCl extractions. The band assigned to the Si-O bond asymmetric stretching was shifted towards higher wavenumbers after both chemical extractions. However, the displacement was more pronounced in AA-WBA binders (≈1060 cm^{-1}) than in WBA (1027 cm^{-1}), due to the formation of new CSH/CASH phases, as can be inferred from the results described in Table 3. In addition, the slight difference in the chemical extractions corroborated the higher amount of CSH and CASH phases in the alkali-activated binders and the lower presence of NASH phases. Likewise, the characteristic peaks in silica gel (≈1050 cm^{-1}, ≈930 cm^{-1}, and ≈790 cm^{-1}) were observed after both chemical extractions. The specimen cured at 85 °C was the only one that had efflorescence on the surface. An analysis of the efflorescence

using the FTIR (Figure 4e) showed bands attributed to the vibrations of the O-C-O bonds, which corroborated the presence of carbonates. The HCl extraction dissolved the carbonate phases present in WBA and AA-WBA binders (Figure 4a–e, respectively), and removed the band around 1436 cm^{-1} and the peak at 875 cm^{-1}, which correspond to the vibrations of the carbonate bonds [20]. However, the SAM extraction did not have a great effect on these vibration frequencies, which corroborated a limited effect on carbonates and a more selective effect on calcareous binder phases (CSH and CASH).

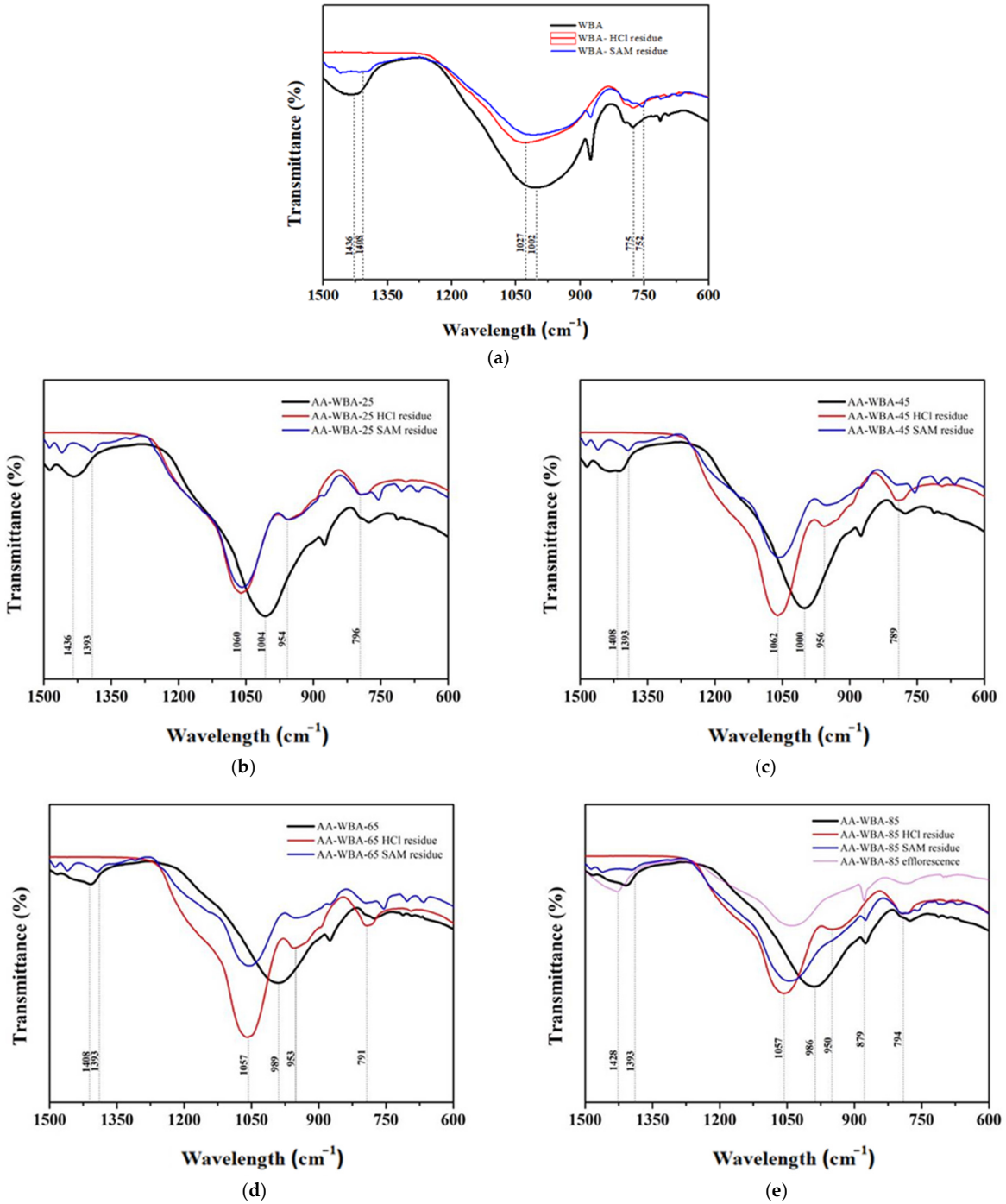

Figure 4. FTIR spectral (1300–800 cm^{-1}) before and after selective chemical extractions: (**a**) WBA > 8 mm; (**b**) AA-WBA-25 °C; (**c**) AA-WBA-45 °C; (**d**) AA-WBA-65 °C; (**e**) AA-WBA-85 °C.

The SEM micrographs of the AA-WBA binders are shown in Figure 5. All microstructures showed the presence of unreacted particles embedded in the binder matrix, which come from the crystalline and poorly reactive phases of the WBA. These unreacted particles probably act as fillers in the material, which results in a micro-mortar-like material. In addition, the specimens cured at temperatures up to 65 °C had a compact appearance (Figure 5a–c), which showed the uniform structure of the binder matrix. However, the specimen cured at 85 °C had a non-homogeneous structure with the formation of disaggregated phases.

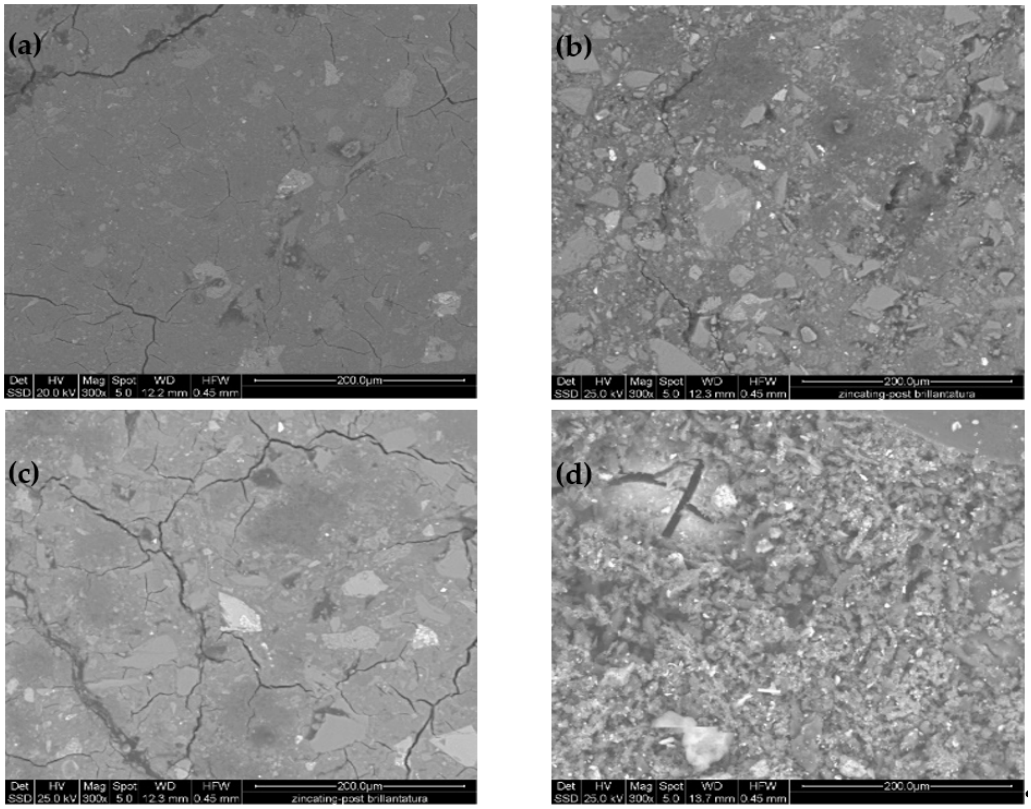

Figure 5. SEM micrograph in the backscattering electron mode of AA-WBA at different curing temperatures: (**a**) AA-WBA-25 °C; (**b**) AA-WBA-45 °C; (**c**) AA-WBA-65 °C; (**d**) AA-WBA-85 °C.

Figure 6 depicts the compressive strength (σ_c) of AA-WBA binders. The difference in compressive strength between specimens cured at 25 °C and 45 °C (13.9 MPa and 14.1 MPa, respectively) was insignificant. The maximum compressive resistance was obtained when curing was performed at 65 °C (29.8 MPa), while a substantial decrease in mechanical performance (21.2 MPa) was observed in the sample cured at 85 °C. This mechanical behavior agrees with the mass dissolved percentage in chemical extractions (see Table 3) and the compact and cohesive structure observed in the sample cured at 65 °C (Figure 5c).

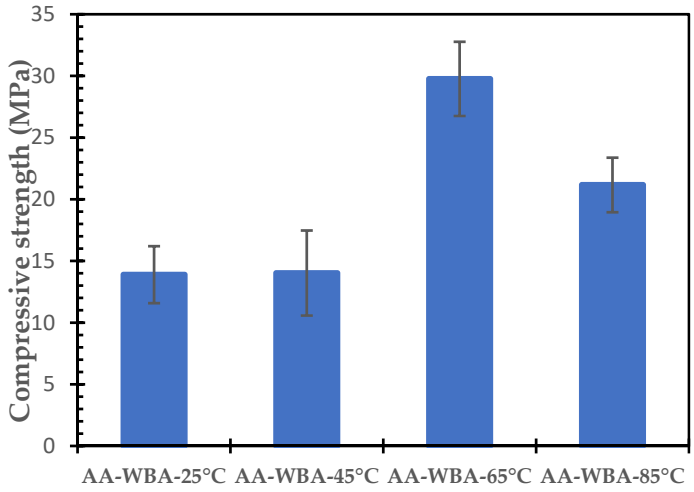

Figure 6. Compressive strength (σ_c) of AA-WBA specimens at different curing temperatures.

A standard leaching test for granular waste materials (EN 12457-4) was performed to assess the potential environmental impact of WBA and AA-WBA binders, simulating the end of their lifecycle. Table 5 summarizes the leaching concentration of heavy metals and metalloids in WBA and different formulations (two replicas per sample). The results obtained were compared with the acceptable limits for waste in landfills (inert, non-hazardous and hazardous) set by the European Union [56]. WBA could be classified as non-hazardous waste since the concentration of antimony (Sb) was above the limit for classification as inert waste. However, no distinct trend was observed in the AA-WBA binders as the curing temperature increased. Small differences in leachate concentration for the same metal could be attributed to the heterogeneity of the precursor, and not to the curing temperature. Most of the heavy metals and metalloids (Ba, Cd, Cu, Cr, Hg, Mo, Pb, Ni, and Zn) remained below the threshold established for classification as non-hazardous waste. Moreover, the concentrations of most of the elements were below the limits for inert materials. By contrast, arsenic (As) and antimony (Sb) exceeded the limits for non-hazardous waste, and even in AA-WBA-65 °C, Sb exceeded the limit for hazardous waste. Both metalloids showed a significant increase in their concentration compared to WBA leachates as a result of the strong alkalinity, together with Ba, Cr, and Zn in smaller measures. The main source of As and Sb derives from the high cullet content in the MSW [13,37], which can dissolve in a strongly alkaline medium, releasing some of these metalloids. The increase in curing temperature does not lead to an improvement in the release of As and Sb, so curing at room temperature seems preferable in terms of the release of both metalloids.

Table 5. Leaching concentration ($mg \cdot kg^{-1}$) in WBA and AA-WBA binders at different curing temperatures after leaching test (EN 12457-4). Curing time: 28 days.

Sample	Ba	As	Cd	Cr	Cu	Hg	Mo	Pb	Ni	Sb	Zn
WBA	0.25	0.23	<0.01	0.17	0.69	0.01	0.33	0.01	0.11	0.27	0.12
AAC-WBA-25 °C	0.44	1.84	<0.01	0.41	0.59	0.01	0.25	0.34	0.07	3.90	0.62
AAC-WBA-45 °C	0.46	2.07	<0.01	0.37	0.57	0.01	0.26	0.29	0.06	4.63	0.41
AAC-WBA-65 °C	0.52	2.85	<0.01	0.43	0.64	<0.01	0.34	0.35	0.06	6.20	0.55
AAC-WBA-85 °C	0.39	1.25	<0.01	0.73	0.85	<0.01	0.16	0.49	0.07	4.32	1.00
[1] Inert Waste	20	0.5	0.04	0.5	2	0.01	0.5	0.5	0.4	0.06	4
[1] Non-hazardous waste	100	2	1	10	50	0.2	10	10	10	0.7	50
[1] Hazardous waste	300	25	5	70	100	2	30	50	40	5	200

[1] Limit for acceptance at landfills [56].

The leaching test for the AA-WBA-65 °C specimen was repeated after 105 days to evaluate the effect of curing time on leaching concentration. Table 6 shows that the increase in curing time led to a significant decrease in the leaching of heavy metals and metalloids, mainly in the case of Sb. Hence, the material is very close to being classified as non-hazardous waste, and only As and Sb were slightly above the established limits. This reduction was probably due to the precipitation and/or adsorption of Sb in the newly formed mineral phases. In this regard, Lancellotti et al. [57] also demonstrated that the increase in curing time of alkali-activated binders formulated with mine tailings led to a decrease in the release of heavy metals and metalloids.

Table 6. Leaching concentration ($mg \cdot kg^{-1}$) of AA-WBA-65 °C binder at different curing times after leaching test (EN12457-4). Curing temperature: 65 °C.

Curing Time	Ba	As	Cd	Cr	Cu	Hg	Mo	Pb	Ni	Sb	Zn
28 days	0.52	2.85	<0.01	0.43	0.64	<0.01	0.34	0.35	0.06	6.20	0.55
105 days	0.30	2.20	0.02	0.20	0.41	<0.01	0.32	0.22	0.02	1.01	0.23

These results corroborate that the final properties of AA-WBA binders are highly dependent on the curing temperature. An increase in curing temperature up to 65 °C enhances the compactness of the binder matrix, produces the maximum compressive strength, and improves the stability of specimens of the binder material. In samples cured at higher temperatures, the mechanical properties decrease slightly, as does the consistency and compactness of the binder matrix. These results are in line with the conclusions proposed by Gebregziabiher et al. [58], who determined that curing at elevated temperature greatly accelerated product formation and increased strength in calcium-rich precursors activated by waterglass solutions. However, a curing temperature close to the boiling temperature of water (i.e., 85 °C) accelerated evaporation of the mixing water, decreased the cohesion of the cementitious phases, and increased porosity (see Figure 5d), with a loss of mechanical properties.

Consequently, the study on the effect of humidity on the curing stage was carried out at a curing temperature of 65 °C.

3.2. Effect of Relative Humidity

A new formulation was developed (AA-WBA-65 °C-CC) that was completely cured in the climatic chamber: first, at 65 °C and 95 ± 2% RH (for 3 days), and subsequently, at 25 °C and 95 ± 2% RH (up to 28 days). The results were compared with those obtained for AA-WBA-65 °C specimens, which were cured in an oven and inside a sealed plastic bag (for 3 days) and then in a climatic chamber (25 °C; 95 ± 2% RH).

No significant differences were observed in the XRD and FTIR characterization of the specimens obtained in both experimental trial formulations. The same crystalline mineral phases were determined (see Table 4) and the most characteristic peaks and bands of AA-WBA (see Figure 3d) were obtained at very similar wavenumbers as well. Therefore, from a qualitative perspective, humidity does not affect the formation of new binder phases (CSH and CASH). However, microstructural differences were observed between both formulations as can be seen in the SEM micrographs of Figure 7. The AA-WBA-65 °C specimen showed lower porosity and a more cohesive microstructure and compact appearance (Figure 7a). In contrast, the AA-WBA-65 °C-CC specimen presented higher porosity and lower cohesion between the binder matrix and the unreacted particles.

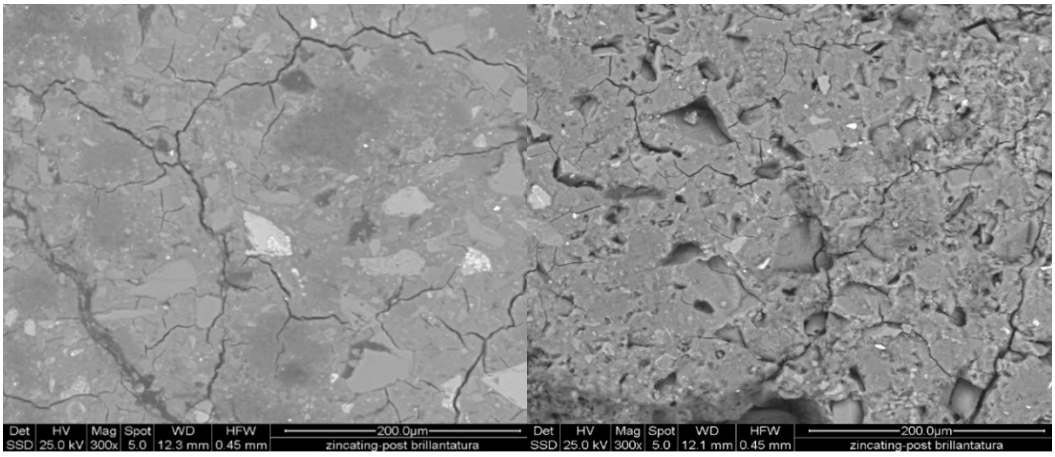

(**a**) (**b**)

Figure 7. SEM micrograph of AA-WBA cured at 65 °C and different humidity conditions: (**a**) AA-WBA-65 °C; (**d**) AA-WBA-65 °C-CC.

These facts were corroborated by determining the density and calculated porosity of the cured specimens in different humidity conditions (Table 7). As expected, AA-WBA-65 °C-CC had higher porosity and lower density than the AA-WBA-65 °C specimen. Considering the equilibrium between water and water vapor ($H_2O_{(l)} \leftrightharpoons H_2O_{(v)}$), a high partial pressure of water vapor (e.g., 95 ± 2% RH) hinders the evaporation of mixing water. The mixing water retained in the bulk will lead to voids in the binder matrix during curing and, consequently, to an increase of porosity. However, low relative humidity in the initial stages of curing (e.g., inside a sealed plastic bag) facilitates the evaporation of mixing water and, therefore, decreases the porosity of the binder material.

Table 7. Density and calculated porosity of the specimens cured at different humidity conditions. Curing temperature: 65 °C.

	AA-WBA-65 °C (Inside Sealed Plastic Bag)	**AA-WBA-65 °C-CC (Climatic Chamber; 95 ± 2% RH)**
Relative density (g·cm^{-3})	2.35	2.21
Apparent density (g·cm^{-3})	1.86	1.68
Porosity (%)	21.00	24.23

The high porosity and low relative density of the AA-WBA-65 °C-CC specimen led to a decrease in compressive strength, as is shown in Figure 8.

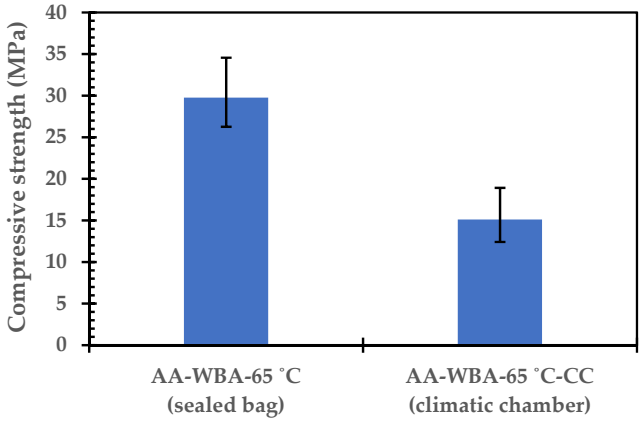

Figure 8. Compressive strength (σ_c) of AA-WBA specimens at different curing humidity. Curing temperature: 65 °C.

Table 8 compares the leaching concentration of heavy metals and metalloids between AA-WBA-65 °C and AA-WBA-65 °C-CC specimens. Low concentrations (except Sb and Zn) were observed in the AA-WBA-65 °C specimen due to its lower porosity. In this regard, higher porosity (i.e., AA-WBA-65 °C-CC) increases the contact surface of the binder material with the leaching medium, which favors the diffusion of heavy metals and metalloids.

Table 8. Leaching concentration ($mg \cdot kg^{-1}$) in AA-WBA-65 °C binder at different curing humidity after leaching test (EN 12457-4). Curing temperature: 65 °C.

	Ba	As	Cd	Cr	Cu	Mo	Pb	Ni	Sb	Zn
AA-WBA-65 °C (sealed plastic bag)	0.52	2.85	<0.01	0.43	0.64	0.34	0.35	0.06	6.20	0.55
AA-WBA-65 °C-CC (climatic chamber)	1.60	4.62	0.20	0.48	0.86	0.66	0.73	0.31	4.39	0.2

4. Conclusions

This research highlights the potential of the coarse fraction of WBA (>8 mm) as the sole precursor used in the formulation of alkali-activated binders. Selective chemical extractions, XRD analysis, and FTIR analysis revealed the presence of CSH and/or CASH gels as the main reaction products that were formed. Although the presence of sodium gels is limited, the formation of (N,C)ASH gels should not be excluded. Likewise, it was determined that a large number of unreacted precursor particles are distributed in the binder matrix, which act as fillers and are similar to those obtained in micro-mortars.

According to the results obtained in this preliminary study, temperature plays a fundamental role during the initial curing process of the alkali-activated binder matrix. As the curing temperature increases, an increase in the compressive strength of the binder material is evidenced. Likewise, a more cohesive and compact microstructure is observed. With the increase in curing temperature, an increase in the percentage of binder phases was also observed, mainly CSH/CASH, whose reaction kinetics were favored by the increase in temperature. However, curing temperatures higher than 65 °C generate the formation of a microstructure of agglomerates that are not very cohesive, with a significant loss of compressive strength.

For the same curing temperature, humidity also played an important role in the final properties of the alkali-activated binder. The equilibrium between water and water vapor regulated the removal of mixing water. A high partial pressure of water vapor (high relative humidity) prevents the evaporation of the mixing water, which is retained in the binder matrix and generates greater porosity. As a result, as porosity increases, compressive strength decreases, and the diffusion and release of metals and metalloids contained in the precursor into the environment increases.

Regarding the potential release of metals and metalloids, for the same relative humidity, it was found that is not significantly affected by the curing temperature. However, lower porosity and a longer curing time considerably decrease the leaching potential of alkaline-activated binders formulated using WBA > 8 mm as the only precursor.

Author Contributions: Conceptualization, A.M.-A., C.L., I.L. and J.M.C.; methodology, P.C.D.T., A.M.-A., J.M. and J.M.C.; formal analysis, P.C.D.T., A.M.-A., J.M. and A.C.Q.-P.; investigation, P.C.D.T. and A.M.-A.; resources, A.M.-A. and J.M.C.; writing—original draft preparation, P.C.D.T. and J.M.C.; writing—review and editing, J.M.C., A.M.-A., J.M., A.C.Q.-P., C.L. and I.L.; supervision, C.L., I.L. and J.M.C.; project administration, J.M.C.; funding acquisition, C.L., I.L. and J.M.C. All authors have read and agreed to the published version of the manuscript.

Funding: This research was partially funded by the Spanish Government (BIA2017-83912-C2-1-R). Pietro C.D. Tortora is grateful to the ERASMUS+ traineeship program for partially financing his stay at the University of Barcelona (43/MO 2019/2020). Alex Maldonado-Alameda and Jofre Mañosa are also grateful to the Agència de Gestió d'Ajuts Universitaris i de Recerca for their research grants, FI-DGR 2017 and FI-2020, respectively.

Institutional Review Board Statement: Not applicable.

Informed Consent Statement: Not applicable.

Data Availability Statement: Not applicable.

Acknowledgments: The authors would like to thank the Agència de Gestió d'Ajuts Universitaris i de Recerca for the quality accreditation given to their research groups DIOPMA (2017 SGR 118). The authors also want to thank SIRUSA and VECSA for supplying the MSWI bottom ash. The authors are grateful to Joseh Cross for English-language revision.

Conflicts of Interest: The authors declare no conflict of interest.

Abbreviations

AAB	alkali-activated binder
AA-WBA	weathered bottom ash-based alkali-activated binders
APC	air pollution control residues
ATR	attenuated total reflectance mode
CASH	calcium aluminosilicate hydrate
CSH	calcium silicate hydrate
FA	coal fly ash
FTIR	Fourier transform infrared spectroscopy
GBFS	granular blast furnace slag
IBA	incineration bottom ash
ICP-MS	inductively coupled plasma mass spectrometry
MK	metakaolin
MSW	municipal solid waste
NASH	sodium aluminosilicate hydrate
PC	Portland cement
RH	relative humidity
SAM	salicylic acid/methanol
SEM	scanning electron microscopy
WBA	weathered bottom ash
WtE	waste-to-energy facilities
XRD	X-ray diffraction
XRF	X-ray fluorescence

References

1. Andrew, R.M. Global CO_2 emissions from cement production. *Earth Syst. Sci. Data* **2018**, *10*, 195–217. [CrossRef]
2. Duxson, P.; Provis, J.L.; Lukey, G.C.; van Deventer, J.S.J. The role of inorganic polymer technology in the development of "green concrete". *Cem. Concr. Res.* **2007**, *37*, 1590–1597. [CrossRef]
3. Provis, J.L.; Van Deventer, J.S.J. *Alkali Activated Materials*; Provis, J.L., Van Deventer, J.S.J., Eds.; Springer: Berlin/Heidelberg, Germany, 2014; Volume 1, ISBN 978-94-007-7671-5.
4. Provis, J.L.; Bernal, S.A. Geopolymers and related alkali-activated materials. *Annu. Rev. Mater. Res.* **2014**, *44*, 299–327. [CrossRef]
5. Puligilla, S.; Mondal, P. Co-existence of aluminosilicate and calcium silicate gel characterized through selective dissolution and FTIR spectral subtraction. *Cem. Concr. Res.* **2015**, *70*, 39–49. [CrossRef]
6. Garcia-Lodeiro, I.; Palomo, A.; Fernández-Jiménez, A.; MacPhee, D.E. Compatibility studies between N-A-S-H and C-A-S-H gels. Study in the ternary diagram Na_2O-CaO-Al_2O3-SiO_2-H_2O. *Cem. Concr. Res.* **2011**, *41*, 923–931. [CrossRef]
7. Haha, M.B.; Lothenbach, B.; Le Saout, G.; Winnefeld, F. Influence of slag chemistry on the hydration of alkali-activated blast-furnace slag—Part II: Effect of Al_2O. *Cem. Concr. Res.* **2012**, *42*, 74–83. [CrossRef]
8. Fernández-Jiménez, A.; Palomo, A. Composition and microstructure of alkali activated fly ash binder: Effect of the activator. *Cem. Concr. Res.* **2005**, *35*, 1984–1992. [CrossRef]
9. De Vargas, A.S.; Dal Molin, D.C.C.; Vilela, A.C.F.; Da Silva, F.J.; Pavão, B.; Veit, H. The effects of Na_2O/SiO_2 molar ratio, curing temperature and age on compressive strength, morphology and microstructure of alkali-activated fly ash-based geopolymers. *Cem. Concr. Compos.* **2011**, *33*, 653–660. [CrossRef]
10. Pacheco-Torgal, F.; Labrincha, J.; Leonelli, C.; Palomo, A.; Chindaprasit, P. *Handbook of Alkali-Activated Cements, Mortars and Concretes*; Elsevier: Amsterdam, The Netherlands, 2014.
11. Song, Q.; Li, J.; Zeng, X. Minimizing the increasing solid waste through zero waste strategy. *J. Clean. Prod.* **2015**, *104*, 199–210. [CrossRef]

12. Cheng, H.; Hu, Y. Municipal solid waste (MSW) as a renewable source of energy: Current and future practices in China. *Bioresour. Technol.* **2010**, *101*, 3816–3824. [CrossRef]
13. Del Valle-Zermeño, R.; Gómez-Manrique, J.; Giro-Paloma, J.; Formosa, J.; Chimenos, J.M. Material characterization of the MSWI bottom ash as a function of particle size. Effects of glass recycling over time. *Sci. Total Environ.* **2017**, *581–582*, 897–905. [CrossRef]
14. Blasenbauer, D.; Huber, F.; Lederer, J.; Quina, M.J.; Blanc-Biscarat, D.; Bogush, A.; Bontempi, E.; Blondeau, J.; Chimenos, J.M.; Dahlbo, H.; et al. Legal situation and current practice of waste incineration bottom ash utilisation in Europe. *Waste Manag.* **2020**, *102*, 868–883. [CrossRef]
15. Zheng, L.; Wang, C.; Wang, W.; Shi, Y.; Gao, X. Immobilization of MSWI fly ash through geopolymerization: Effects of water-wash. *Waste Manag.* **2011**, *31*, 311–317. [CrossRef]
16. Scarlat, N.; Fahl, F.; Dallemand, J.-F. Status and opportunities for energy recovery from municipal solid waste in Europe. *Waste Biomass Valoriz.* **2019**, *10*, 2425–2444. [CrossRef]
17. Geng, Y.; Ji, W.; Wang, Z.; Lin, B.; Zhu, Y. A review of operating performance in green buildings: Energy use, indoor environmental quality and occupant satisfaction. *Energy Build.* **2019**, *183*, 500–514. [CrossRef]
18. Chen, Z.; Liu, Y.; Zhu, W.; Yang, E.H. Incinerator bottom ash (IBA) aerated geopolymer. *Constr. Build. Mater.* **2016**, *112*, 1025–1031. [CrossRef]
19. Maldonado-Alameda, A.; Giro-Paloma, J.; Svobodova-Sedlackova, A.; Formosa, J.; Chimenos, J.M. Municipal solid waste incineration bottom ash as alkali-activated cement precursor depending on particle size. *J. Clean. Prod.* **2020**, *242*, 118443. [CrossRef]
20. Maldonado-Alameda, A.; Giro-Paloma, J.; Alfocea-Roig, A.; Formosa, J.; Chimenos, J.M. Municipal solid waste incineration bottom ash as sole precursor in the alkali-activated binder formulation. *Appl. Sci.* **2020**, *10*, 4129. [CrossRef]
21. Maldonado-Alameda, A.; Mañosa, J.; Formosa, J.; Giro-Paloma, J.; Chimenos, J.M. Alkali-activated binders using bottom ash from waste-to-energy plants and aluminium recycling waste. *Appl. Sci.* **2021**, *11*, 3840. [CrossRef]
22. Maldonado-Alameda, A.; Giro-Paloma, J.; Mañosa, J.; Formosa, J.; Chimenos, J.M. Alkali-activated binders based on the coarse fraction of municipal solid waste incineration bottom ash. *Bol. Soc. Esp. Ceram. Vidr.* 2021; *in press*. [CrossRef]
23. Wei, Y.; Shimaoka, T.; Saffarzadeh, A.; Takahashi, F. Mineralogical characterization of municipal solid waste incineration bottom ash with an emphasis on heavy metal-bearing phases. *J. Hazard. Mater.* **2011**, *187*, 534–543. [CrossRef] [PubMed]
24. Kurda, R.; Silva, R.V.; de Brito, J. Incorporation of alkali-activated municipal solid waste incinerator bottom ash in mortar and concrete: A critical review. *Materials* **2020**, *13*, 3428. [CrossRef] [PubMed]
25. Cho, B.H.; Nam, B.H.; An, J.; Youn, H. Municipal solid waste incineration (MSWI) ashes as construction materials—A review. *Materials* **2020**, *13*, 3143. [CrossRef] [PubMed]
26. Zhu, W.; Teoh, P.J.; Liu, Y.; Chen, Z.; Yang, E.-H. Strategic utilization of municipal solid waste incineration bottom ash for the synthesis of lightweight aerated alkali-activated materials. *J. Clean. Prod.* **2019**, *235*, 603–612. [CrossRef]
27. Polettini, A.; Pomi, R.; Carcani, G. The effect of Na and Ca salts on MSWI bottom ash activation for reuse as a pozzolanic admixture. *Resour. Conserv. Recycl.* **2005**, *43*, 403–418. [CrossRef]
28. Onori, R.; Will, J.; Hoppe, A.; Polettini, A.; Pomi, R.; Boccaccini, A.R. Bottom ash-based geopolymer materials: Mechanical and environmental properties. *Ceram. Eng. Sci. Proc.* **2011**, *32*, 71–82.
29. Lancellotti, I.; Ponzoni, C.; Bignozzi, M.C.; Barbieri, L.; Leonelli, C. Incinerator bottom ash and ladle slag for geopolymers preparation. *Waste Biomass Valoriz.* **2014**, *5*, 393–401. [CrossRef]
30. Lancellotti, I.; Cannio, M.; Bollino, F.; Catauro, M.; Barbieri, L.; Leonelli, C. Geopolymers: An option for the valorization of incinerator bottom ash derived "end of waste". *Ceram. Int.* **2015**, *41*, 2116–2123. [CrossRef]
31. Garcia-Lodeiro, I.; Donatello, S.; Fernández-Jiménez, A.; Palomo, Á. Hydration of hybrid alkaline cement containing a very large proportion of fly ash: A descriptive model. *Materials* **2016**, *9*, 605. [CrossRef]
32. Wongsa, A.; Boonserm, K.; Waisurasingha, C.; Sata, V.; Chindaprasirt, P. Use of municipal solid waste incinerator (MSWI) bottom ash in high calcium fly ash geopolymer matrix. *J. Clean. Prod.* **2017**, *148*, 49–59. [CrossRef]
33. Huang, G.; Yuan, L.; Ji, Y.; Liu, B.; Xu, Z. Cooperative action and compatibility between Portland cement and MSWI bottom ash alkali-activated double gel system materials. *Constr. Build. Mater.* **2019**, *209*, 445–453. [CrossRef]
34. Huang, G.; Yang, K.; Sun, Y.; Lu, Z.; Zhang, X.; Zuo, L.; Feng, Y.; Qian, R.; Qi, Y.; Ji, Y.; et al. Influence of NaOH content on the alkali conversion mechanism in MSWI bottom ash alkali-activated mortars. *Constr. Build. Mater.* **2020**, *248*, 118582. [CrossRef]
35. Chen, B.; Brito van Zijl, M.; Keulen, A.; Ye, G. Thermal treatment on MSWI bottom ash for the utilisation in alkali activated materials. *KnE Eng.* **2020**, *2020*, 25–35. [CrossRef]
36. Piccolo, F.; Andreola, F.; Barbieri, L.; Lancellotti, I. Synthesis and characterization of biochar-based geopolymer materials. *Appl. Sci.* **2021**, *11*, 10945. [CrossRef]
37. Maldonado-Alameda, A.; Giro-Paloma, J.; Rodríguez-Romero, A.; Serret, J.; Menargues, A.; Andrés, A.; Chimenos, J.M. Environmental potential assessment of MSWI bottom ash-based alkali-activated binders. *J. Hazard. Mater.* **2021**, *416*, 125828. [CrossRef] [PubMed]
38. Carvalho, R.; Silva, R.V.; de Brito, J.; Pereira, M.F.C. Alkali activation of bottom ash from municipal solid waste incineration: Optimization of NaOH- and Na $2SiO_3$-based activators. *J. Clean. Prod.* **2021**, *291*, 125930. [CrossRef]
39. Jin, L.; Huang, G.; Li, Y.; Zhang, X.; Ji, Y.; Xu, Z. Positive influence of liquid sodium silicate on the setting time, polymerization, and strength development mechanism of mswi bottom ash alkali-activated mortars. *Materials* **2021**, *14*, 1927. [CrossRef] [PubMed]

40. Bernal, S.A.; Mejía de Gutiérrez, R.; Pedraza, A.L.; Provis, J.L.; Rodriguez, E.D.; Delvasto, S. Effect of binder content on the performance of alkali-activated slag concretes. *Cem. Concr. Res.* **2011**, *41*, 1–8. [CrossRef]
41. Gebregziabiher, B.S.; Thomas, R.; Peethamparan, S. Very early-age reaction kinetics and microstructural development in alkali-activated slag. *Cem. Concr. Compos.* **2015**, *55*, 91–102. [CrossRef]
42. Aydın, S.; Baradan, B. Mechanical and microstructural properties of heat cured alkali-activated slag mortars. *Mater. Des.* **2012**, *35*, 374–383. [CrossRef]
43. Altan, E.; Erdoğan, S.T. Alkali activation of a slag at ambient and elevated temperatures. *Cem. Concr. Compos.* **2012**, *34*, 131–139. [CrossRef]
44. Bandarra, B.S.; Pereira, J.L.; Martins, R.C.; Maldonado-Alameda, A.; Chimenos, J.M.; Quina, M.J. Opportunities and barriers for valorizing waste incineration bottom ash: Iberian countries as a case study. *Appl. Sci.* **2021**, *11*, 9690. [CrossRef]
45. Zhu, W.; Chen, X.; Struble, L.J.; Yang, E.H. Characterization of calcium-containing phases in alkali-activated municipal solid waste incineration bottom ash binder through chemical extraction and deconvoluted Fourier transform infrared spectra. *J. Clean. Prod.* **2018**, *192*, 782–789. [CrossRef]
46. Lodeiro, I.G.; Macphee, D.E.; Palomo, A.; Fernández-jiménez, A. Effect of alkalis on fresh C-S-H gels. FTIR analysis. *Cem. Concr. Res.* **2009**, *39*, 147–153. [CrossRef]
47. Fernández-Jiménez, A.; Palomo, A. Mid-infrared spectroscopic studies of alkali-activated fly ash structure. *Microporous Mesoporous Mater.* **2005**, *86*, 207–214. [CrossRef]
48. Alonso, S.; Vázquez, T.; Puertas, F.; Martínez-Ramírez, S. Alkali-activated fly ash/slag cement strength behaviour and hydration products. *Cem. Concr. Res.* **2000**, *30*, 1625–1632.
49. Huang, G.; Ji, Y.; Li, J.; Zhang, L.; Liu, X.; Liu, B. Effect of activated silica on polymerization mechanism and strength development of MSWI bottom ash alkali-activated mortars. *Constr. Build. Mater.* **2019**, *201*, 90–99. [CrossRef]
50. Ping, Y.; Kirkpatrick, R.J.; Brent, P.; McMillan, P.F.; Xiandong, C. Structure of calcium silicate hydrate (C-S-H): Near-, mid-, and far-infrared spectroscopy. *J. Am. Ceram. Soc.* **1999**, *82*, 742–748.
51. Criado, M.; Palomo, A.; Fernández-Jiménez, A. Alkali activation of fly ashes. Part 1: Effect of curing conditions on the carbonation of the reaction products. *Fuel* **2005**, *84*, 2048–2054. [CrossRef]
52. Fernández-Jiménez, A.; Puertas, F.; Sobrados, I.; Sanz, J. Structure of calcium silicate hydrates formed in alkaline-activated slag: Influence of the type of alkaline activator. *J. Am. Ceram. Soc.* **2003**, *86*, 1389–1394. [CrossRef]
53. Puertas, F.; Fernández-Jiménez, A.; Blanco-Varela, M.T. Pore solution in alkali-activated slag cement pastes. Relation to the composition and structure of calcium silicate hydrate. *Cem. Concr. Res.* **2004**, *34*, 139–148. [CrossRef]
54. García-Lodeiro, I.; Fernández-Jiménez, A.; Blanco, M.T.; Palomo, A. FTIR study of the sol-gel synthesis of cementitious gels: C-S-H and N-A-S-H. *J. Sol Gel Sci. Technol.* **2008**, *45*, 63–72. [CrossRef]
55. Criado, M.; Fernández-Jiménez, A.; Palomo, A. Alkali activation of fly ash: Effect of the SiO_2/Na_2O ratio. Part I: FTIR study. *Microporous Mesoporous Mater.* **2007**, *106*, 180–191. [CrossRef]
56. Council of the European Union. 2003/33/EC Council Decision Establishing Criteria and Procedures for the Acceptance of Waste at Landfills Pursuant to Article 16 of and Annex II to Directive 1999/31/EC. Available online: https://eur-lex.europa.eu/legal-content/GA/TXT/?uri=celex:32003D0033 (accessed on 13 December 2021).
57. Lancellotti, I.; Catauro, M.; Dal, F.; Kiventer, J.; Leonelli, C.; Illikainen, M. Alkali activation as new option for gold mine tailings inertization. *J. Clean. Prod.* **2018**, *187*, 76–84.
58. Gebregziabiher, B.S.; Thomas, R.J.; Peethamparan, S. Temperature and activator effect on early-age reaction kinetics of alkali-activated slag binders. *Constr. Build. Mater.* **2016**, *113*, 783–793. [CrossRef]